applied sciences

MDPI

Article

Degradation products on Byzantine glasses from Northern Tunisia

Valeria Comite [1], Martina Andreoli [2], Davide Atzei[3], Donatella Barca[4], Marzia Fantauzzi[3], Mauro Francesco La Russa[4], Antonella Rossi[3], Vittoria Guglielmi[1] and Paola Fermo [1*]

[1] Dipartimento di Chimica, Università degli Studi di Milano, Via Golgi 19, 20133, Milano
[2] Dipartimento di Lettere e Filosofia, Università degli Studi di Trento, Via Tommaso Gar 14, Trento
[3] Università degli Studi di Cagliari, Dipartimento di Scienze Chimiche e Geologiche, S.S. 554 bivio per Sestu, Monserrato (Cagliari)
[4] Dipartimento di Biologia, Ecologia e Scienze della Terra (DiBEST), Università della Calabria, Via Pietro Bucci, 87036 Arcavacata di Rende (Cs)
* Correspondence: paola.fermo@unimi.it

Received: date; Accepted: date; Published: date

Abstract

This study deals with the identification of the degradation products present on some Byzantine glasses coming from an archaeological excavation in Northern Tunisia. The main purpose of the present investigation is the identification of the products and the characterization of surface altered points, namely iridescent and black patinas, which are present on some selected glasses. Non-destructive techniques such as XPS (X-ray photoelectron spectroscopy), SEM-EDS (scanning electron microscopy coupled with energy dispersive X-ray analysis), ATR-FTIR (Attenuated Total Reflection - Fourier Infrared Spectroscopy) and LA-ICP-MS (laser-ablation Inductively Coupled Plasma – Mass Spectrometry) are here exploited. SEM-EDS was employed to ascertain the morphological structure and the chemical composition of various points, apparently different, on the glass surfaces. Small area XPS was performed for identifying the elements present on the sample surface, for determining their chemical state and for establishing the atomic composition of the morphologically different regions. LA-ICP-MS was exploited aiming to determine the chemical composition as far as the trace elements is concerned and trace elements. The presence of iridescent patinas and of encrustations has been highlighted on the glass surfaces in correspondence of the altered areas: iridescent patinas are due to the fact that the glasses are depleted in alkali and alkaline earths. The incrustations resulted to be due to the presence of calcium carbonates, and/or oxyhydoxides. In one case sulphides were also detected by SEM.

Keywords: Byzantine glass; degradation products; patinas; XPS; LA/ICP-MS; SEM-EDS; FTIR

1. Introduction

A very interesting aspect concerning archaeological glass analysis is represented by the study of the degradation and corrosion processes [1-7]. Surface alteration is due to burial conditions and depends on different parameters such as temperature, humidity, pH [8] glass-composition and pollution. In particular, both soil and groundwater compositions, if the objects were buried, play an important role in the glass degradation phenomena. Other factors include the exposure time, the temperature

(especially fluctuating temperatures), the amount of water in contact with the surface, and the alkalinity or acidity of the burial environment [8-9]. It has also been demonstrated that archaeological glass objects found in dry soils are better preserved than those found in moist soils, as water is acknowledged to be one of the main causes of glass weathering [9].

Furthermore, the stability of an ancient glass is even worse due to the presence of elements such as alkali and alkaline earths, which have weaker bonds to oxygen within the glass network [10-11].

Among the glass constituents, sodium carbonate decahydrate (natron) or plant ash were used as fluxes by glassmakers to lower the temperature at which the silica melts. The fluxes (sodium or potassium compounds) are ionically bound into the glass network and reduce the glass viscosity, and alkaline earth metals such as calcium and magnesium, which make the glass more durable [12-13]

Dealkalinized layers i.e. surface layers with a lower concentration of alkali and alkaline earths ions than underneath, constitute the common degradation pathology, which develops on the surface of buried glasses [6].

It is the alkali that is normally primarily lost from the glass surface upon initial corrosion [9].

In particular ion-exchange reactions between hydrogen-bearing species of the attacking liquid and the alkali ions present in the glass, take place causing a depletion of these species in the outermost layers.

The main forms of degradation that occurs are:

i) formation on the surface of an iridescent patina that affects only the outermost layers, produced by the changed reflection conditions of the light due to the presence of the exfoliated surface [11, 14-19];

ii) formation on the surface of crusts, that makes the glass opaque and determines a decrease in gloss; the alteration layers modified the surface appearance . A pearly stratification forms on the surface, which tends to fragment over time [11, 20-27].

The alkaline and alkaline earth metals form weak ionic bonds with the network oxygen and are replaced by H+ ions of the aqueous solution.

In particular the first step consists on the ion-exchange of the glass alkaline ions (M+ = Na+ and sometimes K+) with H+ ions from water [6].

$$SiOM + H_3O^+ \rightarrow SiOH + M^+ + H_2O$$

As a consequence, within the network a depletion of alkali ions (Na^+ and K^+) and alkaline earths ions and an enrichment of hydrated silica (i.e. a layer without alkali is formed on the surface) are observable. This is a diffusive phenomenon that only involves the outermost layers and depends a lot on the composition of the glass. In general, K^+ ions exchange much more easily than Na + ions and both tend to exchange even more easily than alkaline earth ions.

The new layers formed are often brittle and can be easily detached even by small mechanical or friction impacts.

All these alterations partly result from the action of adsorbed water on the glass surfaces and partly from the deposition of other atmospheric components. In the early stages of exposure, alteration consists mainly of the crystallization of salts on the glass surface, referred to as neocrystallisations [5,7,21]. These neocrystallisations result from the reaction between the anions and the cations present in the water or in the atmosphere in the contact with the glass. [5].

In a previous paper we have thoroughly investigated by means of numerous analytical techniques [28] a group of Roman and Byzantine glass shards collected during an excavation campaign at Aïn Wassel in the surroundings of the ancient city of Thugga in northern Tunisia [29-30], a territory belonged to the Roman province of *Africa Proconsularis* and particularly flourishing during the Roman and Byzantine periods. The study has been carried out with the aim to chemically characterize the objects to study the production technology including the chromophores responsible for the different color shades.

The main constituents used for ancient glass fabrication were the raw material, the flux and the coloring agents. As far as Thugga's glasses, for the raw materials a local origin of the sand has been hypothesized due to the homogeneity of the samples from the compositional point of view and in accordance with the presence of sand deposits of important rivers of that area. Concerning the flux in most of the cases a mixture of natron and plant ash was used [28].

As regards the glass chemical composition, it was found [28] that the chemical elements responsible for the different glass shades were generally Fe for the green shades, copper and cobalt for the blue ones, manganese (used as discoloring agent) for the colorless samples. Roman and Byzantine glasses generally show a good standard of technology, particularly in terms of color control. Transition metal ions, such as iron (Fe^{3+}/Fe^{2+}), cobalt (Co^{2+}) and copper (Cu^{2+}/Cu^{+}) acted as coloring agents.
In the present work we have investigated the degradation and corrosion products present on the surface of some of these shards. To ascertain the composition of the glass surfaces the analyses have been carried out by means of techniques such as small area XPS (X-ray photoelectron spectroscopy), SEM-EDS (scanning electron microscopy coupled with energy dispersive X-ray analysis), ATR-FTIR (Attenuated Total Reflection - Fourier Infrared Spectroscopy) and laser-ablation ICP-MS (Inductively Coupled Plasma – Mass Spectrometry).

2. Materials and Methods

The investigated samples belong to the small finds of the University of Trento's excavation of the Late Antique – Byzantine farm at Aïn Wassel (or Ouassel) in Northern Tunisia (ancient Africa Proconsularis), carried out between 1994 and 1996. The vast site is located at 530 m asl on the southern slope of a hill, in the surroundings of the well-known city of Thugga. During fieldwork, 132 glass fragments have been collected, representing approximately 1% of the discovered archaeological material. The shards could be associated to 56 different glass forms or objects, partly dating to the late 4th and 5th century A.D. and partly to the 6th-7th century A.D. [29-30] In this work some samples belonging to stemmed goblets and to a toed lamp from the latter period have been selected and are reported in table 1 and Fig. 1. All the glasses presented on the surface some areas where evident alterations were present. The analytical techniques employed for the characterization of each sample are also listed.

Table 1. Analyzed glass samples: together with the color, the analytical techniques employed for the characterization of each sample, are here listed.

Sample identification	color	analytical techniques
GLR011 (sample n.24 in [28])	light yellow	SEM-EDS, small-area XPS
GLU034 (R14-U209, not included in [28])	light blue	SEM-EDS, LA-ICP-MS
GLB002 (sample n.39 in [28])	colorless-light blue	SEM-EDS, FT-IR, small-area XPS, LA-ICP-MS
GLR014 (sample n.22 in [28])	yellowish	SEM-EDS, small-area XPS

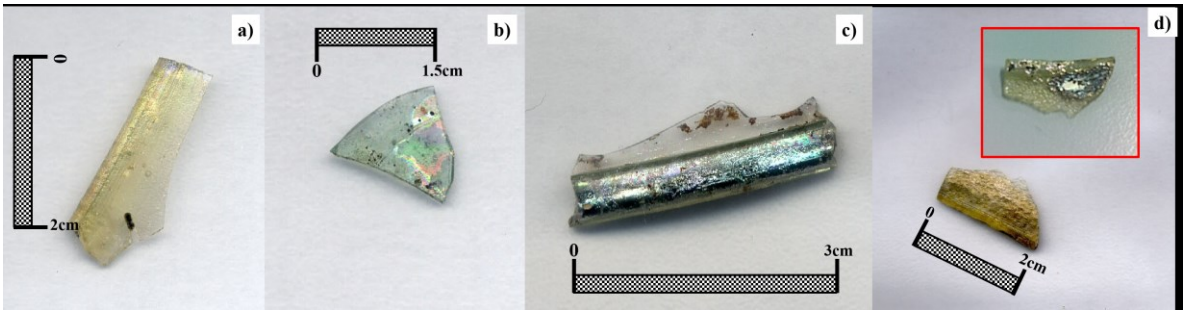

Figure 1. Samples GLR011 a) and GLU034 b) and GLB002 c) and d) GLR014 showing typical degradation layers.

125 2.1 Small-area XPS (Small-area X-ray Photoelectron Spectroscopy)

126 Small-area XPS was performed on selected regions of the sample surface using a monochromatic and
127 focused Al ka X-ray source to determine the elemental chemical composition, the chemical state of
128 the elements and the atomic concentration. The analysis areas were chosen using a microscope
129 mounted on the ultrahigh vacuum chamber and the images were saved together with the XP-spectra.
130 The X-ray spot was of 400 μm and the pass energy was set at 100 eV for the high-resolution spectra
131 and at 200 eV for the survey ones. Under these conditions the full width at half maximum of Ag $3d_{5/2}$
132 recorded on sputtered silver was found to be 0.83 eV when the pass energy was set at 100 eV. A flood
133 gun was used for charging compensation and the binding energy scale was referenced to the
134 adventitious aliphatic at 285.0 eV. More details on experimental set up and data processing are
135 provided in [28].

136

137 2.2 SEM-EDS (Scanning Electron Microscopy coupled with Energy Dispersive X-ray analysis)

138 The glass shards were analyzed by SEM-EDS to obtain qualitative/semiquantitative information on
139 the chemical composition in both unaltered and altered areas. The analyses have been acquired using
140 the ZAF (Z= atomic number; A= self-absorption effect; F= fluorescence effect). During this procedure
141 the data are automatically normalized. For each analysis 3 measurements were performed. The
142 instrument employed was a Hitachi TM1000 equipped with an energy dispersive X-ray spectrometer
143 (Oxford Instruments SwiftED). The images have been acquired at different magnifications while EDS
144 analyses were performed on areas of about 300 x 300 μm. Measurements were directly performed on
145 samples since no metal coating was required according to a procedure previously set up [31].

146 *2.3* ATR-FT-IR (Attenuated Total Reflection - Fourier Infrared Spectroscopy)

147 Infrared spectra were collected on the micro samples by a Nicolet 380 spectrophotometer coupled
148 with ATR accessory Smart Orbit equipped with a diamond crystal. Spectra have been acquired in the
149 range 500–4000 cm^{-1} at a resolution of 4 cm^{-1}.

150

151 2.4 LA-ICP-MS (Laser ablation inductively coupled plasma mass spectrometry)

152

153 Trace element concentrations were carried out using an Inductively Coupled Plasma Mass
154 Spectrometry with Laser Ablation (LA-ICP-MS). The LA-ICP-MS equipment was an Elan DRCe
155 (Perkin Elmer/SCIEX), connected to a New Wave UP213 solid-state Nd-YAG laser probe (213 nm).
156 Samples were ablated by laser beam in a cell, and the vaporized material was then flushed (Gunther
157 & Heinrich 1999) [32] to the ICP, where it was quantified. The procedures for data acquisition were
158 those normally used in the Mass Spectroscopy Laboratory of the Department of Biology, Ecology and
159 Earth Sciences, University of Calabria [33-36].
160 Two different types of analyses were executed on each fragment. Using an ablation crater of 50 μm
161 in diameter and 70/80 μm in depth, three/four spot analyses were carried out on each shard to
162 determine the trace element composition.
163 Then the analyses were executed along an ablation line characterized by a length of about 50 μm and
164 a depth and a width of 5 μm, to determine the trace element composition of degraded areas and to
165 be sure to analyse only the degraded layer. In both cases the ablation time was about 60s.

166

167

168

3. Results

3.1. SEM-EDS

Electron microscopy in combination with energy dispersive X-ray microanalysis has successfully contributed to the investigation of degradation phenomena on materials of art and archaeology [37-39]. In the present study SEM-EDS investigations made possible to highlight mainly two kinds of surface degradation developed on the different samples, i.e. iridescent patinas and crusts.
In table 2 the results of SEM-EDS analysis on samples GLU034, GLR011 and GLB002 are reporter.
GLU034 and GLR011 samples (Fig. 2) appear iridescent in the altered areas. The corresponding elemental analyses, carried out by SEM-EDS, are shown in Fig. 3 for sample GLR011. In the altered areas an enrichment in silica and a depletion in alkali is observable. It is worth nothing that, as already reported in our previous work dealing with the characterization of these glasses [28], low sodium concentrations were in general detected but this is in accordance with other cases reported in the literature as we have underlined in Fermo et al. 2016 [28]. This has been observed for all the samples and it could be probably attributable to some initial depletion in sodium even if visually unaltered areas are clearly observable as it is well evident from the images reported in fig. 1.

Table 2. SEM-EDS semi-quantitative analyses (wt%); for each oxide and element, the percentage is calculated as mean value over three measurements on two different areas of the same sample; for all the detected elements and oxides the standard deviation was lower than 5%.

	GLU0034		**GLR011**		**GLB002**	
	Unaltered glass	**Altered glass iridescent patina**	**Unaltered glass**	**Altered glass iridescent patina**	**Unaltered glass**	**Altered glass external crust**
Na_2O	2.88	2.24	2.26	1.85	2.44	3.24
MgO	1.62	0.56	0.22	-	0.67	1.70
Al_2O_3	1.00	5.82	6.48	7.54	3.32	5.64
SiO_2	75.68	73.17	66.41	76	81.05	42.00
CaO	9.06	9.26	13.32	8.44	6.45	7.98
K2O	4.69	5.42	5.44	1.90	2.70	3.19
TiO_2	1.93	0.84	1.37	1.11	0.00	2.00
Fe_2O_3	1.31	0.90	2.54	1.58	1.60	8.98
MnO	0.57	0.73	-	-	0.00	24.02
Cl	1.25	1.05	1.96	1.58	1.78	1.32
S	-	-	-	-	-	1.20

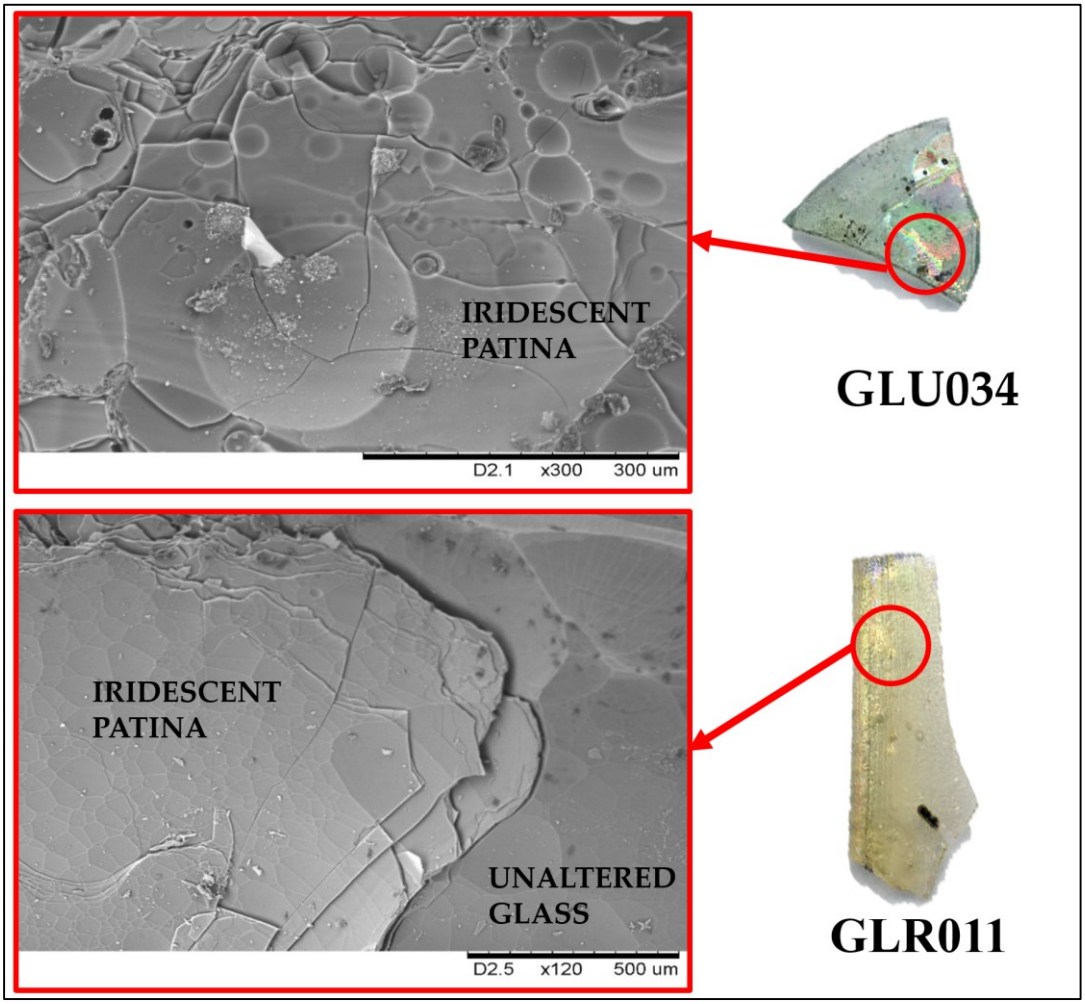

Figure 2. SEM images acquired on the iridescent surface of GLU034 and GLR011 samples.

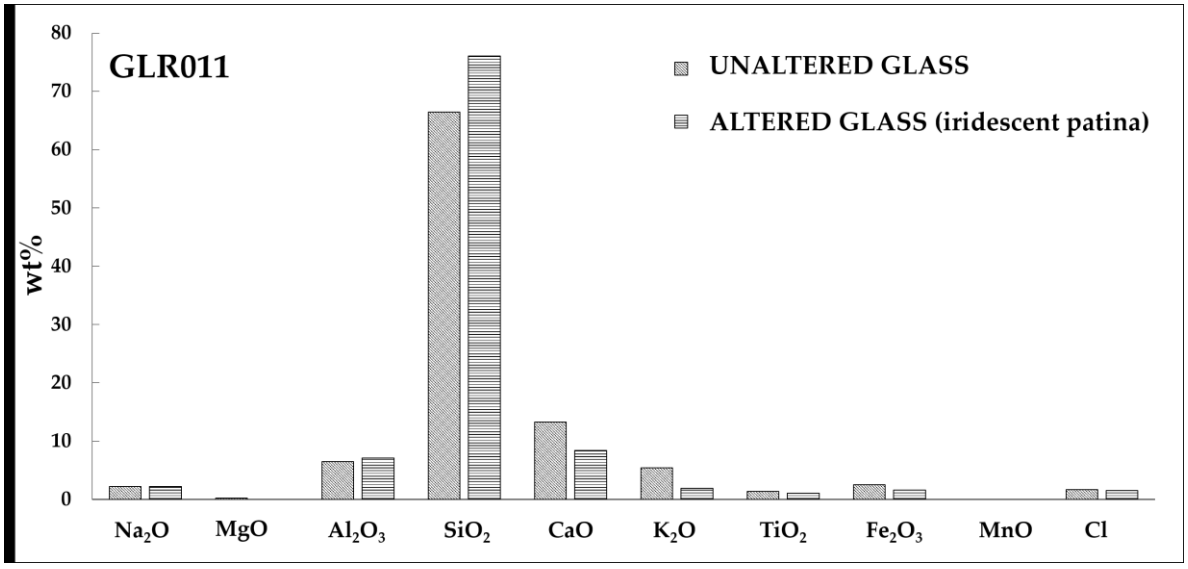

Figure 3. Mean concentrations (wt%) detected by SEM-EDS of the elements present on the altered (iridescent area) and unaltered area of sample GLR011.

A different situation has been observed for sample GLB002 (Fig. 4) that showed on the surface a layer of dark brown encrustations (an iridescent area was also present in this sample, but it was not possible to analyze it by SEM-EDS because of the poor quality of the signal because of the orientation of the surface / electron beam. The alteration phenomenon that we have observed, i. e. iridescent patina and crusts formation on the surfaces of our samples, have been already observed in the literature (see also the description reported in the introduction) [11, 20-27, 40-42].

In this case an opposite situation has been observed with respect to what observed for samples GLR011 and GLU034; in fact, in this case a depletion in silica and an enrichment in alkali is present (Fig. 5). Furthermore, the black encrustations are enriched in titanium, iron and manganese. It is worth to notice that these elements are those typically present in the glass composition [28].

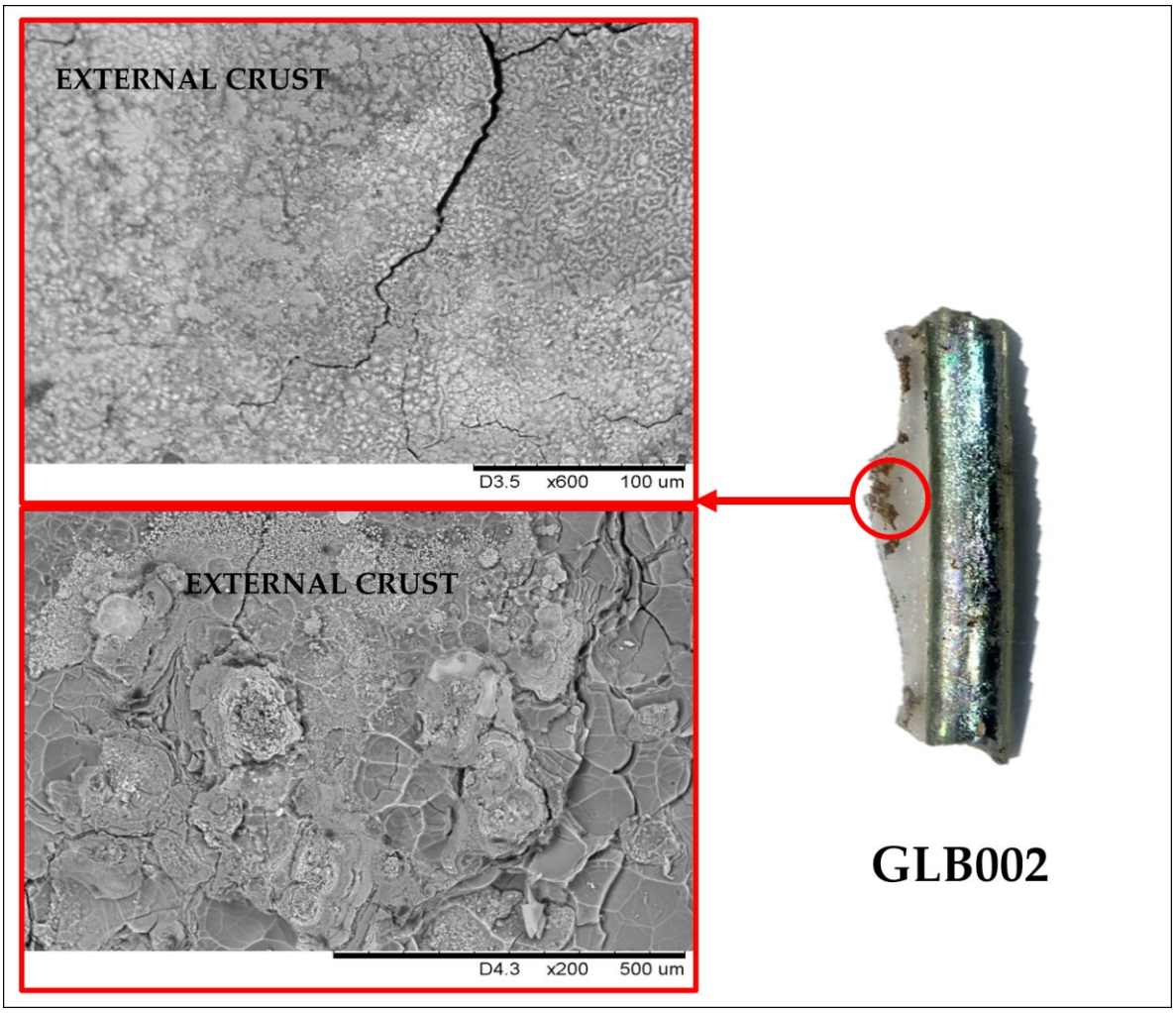

Figure 4. SEM image acquired on the dark-brown area of sample GLB002

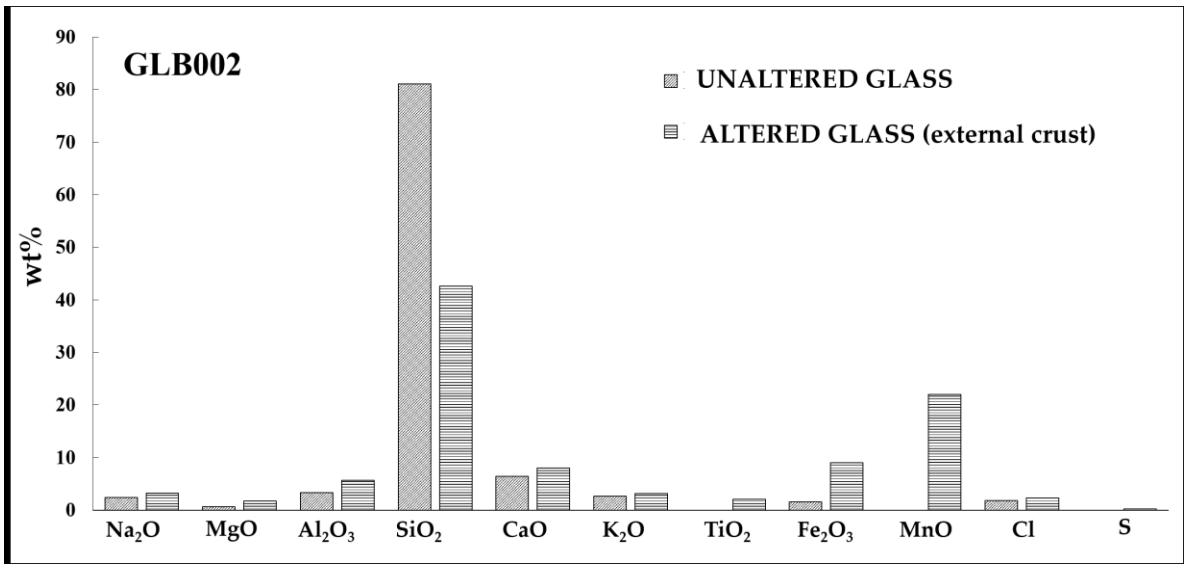

Figure 5. Mean concentrations (wt%) detected by SEM-EDS of the elements present on the unaltered and altered areas (showing the presence of a crust) of sample GLB002.

3.2 FT-IR

ATR-FTIR was used for investigating the incrustations present in the altered areas. As an example, in fig. S.1 (Supplementary Material) the spectra acquired on various regions of sample GLB002 are reported. The typical signals due to $CaCO_3$ at about 1420 and 871 cm^{-1} are present together with some signals of lower intensity at about 2920 cm^{-1} attributable to organic substances (probably due to some contamination from the soil) while at about 1000 cm-1 there is the stretching of Si-O-Si functionality. The broad band between 3600-3400 cm^{-1} were attributed to some water probably absorbed on the surface.

3.3 Small area *XPS*

Samples labeled as GLR014, GLB002 and GLR011 were selected for the present investigation since they show various kind of weathering: iridescence and incrustations. X-ray photoelectron spectroscopy, which is a non-destructive technique, may be operated in various modes and within them small-area XPS was selected in the present investigation. The reason for this choice is that, despite a decrease of the signal intensities, this technique allows gaining chemical information only of the altered regions as well of the regions that morphologically exhibit changes in color or the presence of deposits provided that the analyzed region is at least three times larger than the beam diameter selected for the analysis. In this way, it is possible the characterization of selected regions of the sample and thus a comparison of the composition between morphologically different areas for obtaining information useful in the identification of the degradation process.

Through XPS the surface concentrations of the main chemical elements have been obtained and in particular the oxidation states of the elements, the presence of carbonate salts and concentration trends of some elements in the outermost layers.

As far as GLB002 sample, three different regions were characterized as pointed out in the photographs of Figure 6: point 1 in Fig. 6a, external crust labeled as point 2 in the same figure and an iridescent area (point 3 in Fig. 6a)

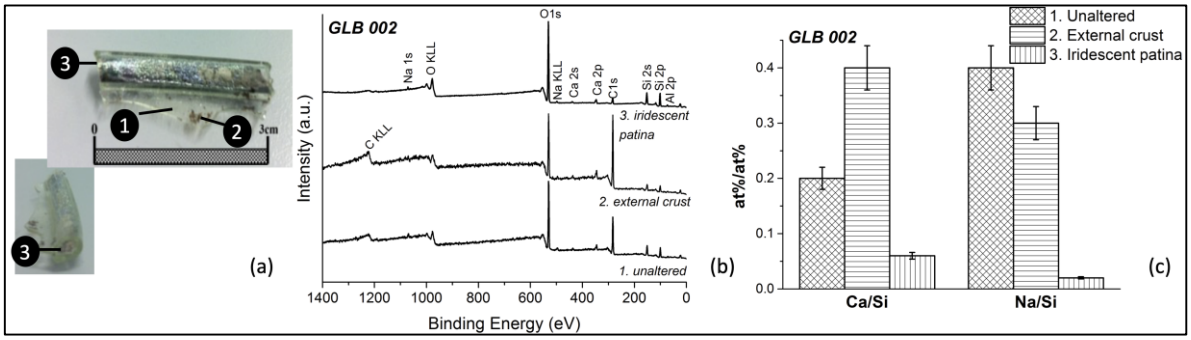

Figure 6. (a) The pictures show the analyzed areas in sample GLB002; (b) It reports X-ray photoelectron survey spectra acquired on the three different areas with a monochromatic Al Kα X-ray source; and c) compares the surface cations-to-silicon ratios.

A detailed inspection of the survey spectra (Fig. 6b) allows the identification of the main constituents of the samples' surfaces. Oxygen, silicon, aluminum, calcium and sodium were detected on the surfaces of all the analyzed areas. Potassium was only revealed in point 1 and small amounts of iron were found on the external crust (point 2) and on the iridescent portion of the sample (point 3) (Fig. 7). A curve fitting of Fe 2p peaks according to [43] was performed and allows observing that in the external crust the % of the peak area ascribed to Fe (II) is lower (13%) than in the iridescent areas (35%).

Surface composition is given in atomic percentage (Table S.1). The external crust and the iridescent patina were clearly depleted in alkali: K is not detected in point 2 and 3 and Na/Si ratio decreases from 0.3 in point 1 to 0.2 in the external crust and; it is found to be 0.03 in the iridescent patina (point 3 Fig. 6c). Ca/Si ratio is higher in the external crust than in the point 1 while it is lower in the iridescent patina.

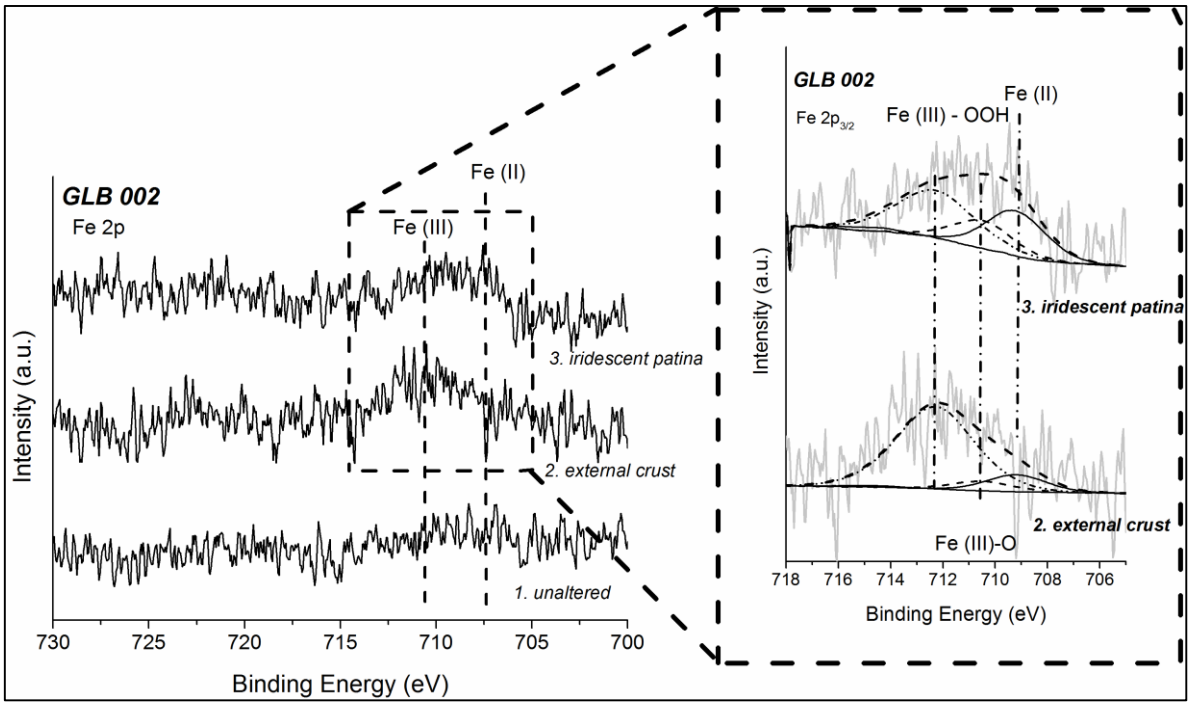

Figure 7. Fe 2p peak obtained on the sample GLB002 in point 1, in the external crust (point 2) and in the iridescent patina (point 3).

Two different regions were analyzed in the **GLR011 sample**: point 1 (unaltered) and point 2 (iridescent patina) in Figure 8a.

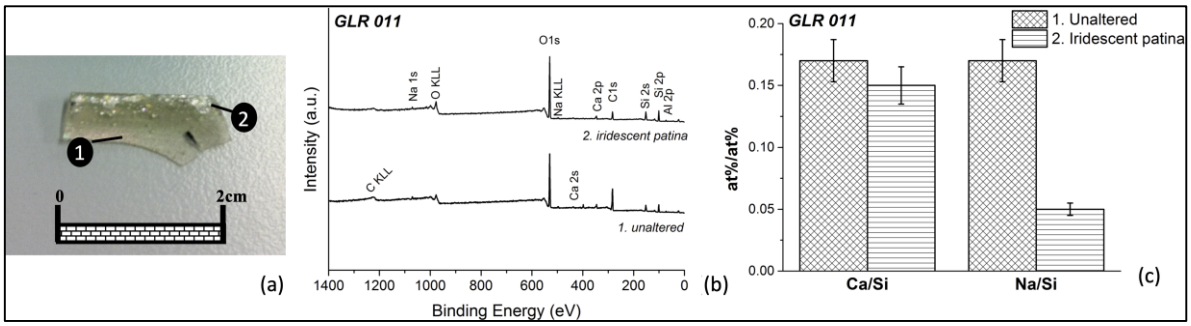

Figure 8. (a) The analyzed areas selected on sample GLR011 are shown in the photograph; (b) The X-ray photoelectron survey spectra acquired on the two different areas with the monochromatic Al Kα X-ray source using a beam of 400μm are compared and (c) the chemical composition provided as surface cations/silicon ratios is presented for the same analysis points.

The detailed surface composition in atomic percentages of the GLR011 sample is reported in Table 2. Si, O, Al, Ca and Si were the only detectable elements together with C. The presence of this element might be ascribed to contamination (Figure 8b). The cations-to-Si ratios showed a pronounced depletion of Na (Figure 8c) in point 2, which exhibits an iridescence compared to point 1 and a minor decrease of Ca/Si ratio.

Also, in the case of sample GLR014 two different areas were characterized, i.e. point 1 and point 2 of Figure 9a.

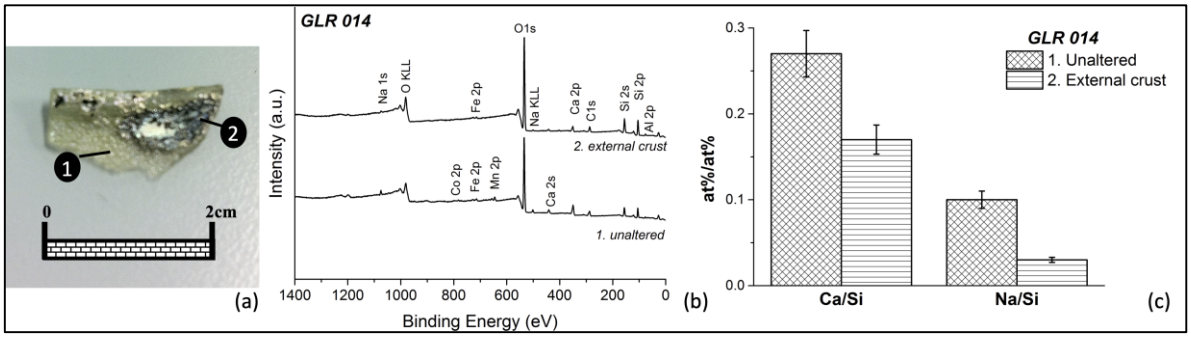

Figure 9. (a) The analyzed areas in sample GLR014 show the regions were the XPS spectra were collected; the corresponding X-ray photoelectron survey spectra acquired on the two different areas with a monochromatic Al Kα X-ray source are shown in (b) together with the surface cations-to-silicon ratios (c).

The inspection of the survey spectra acquired on sample GLR014 allows the identification of iron, cobalt, manganese together with oxygen, silicon, aluminum, sodium and calcium in point 1 of this sample (Fig. 9b); table 2 lists the atomic percentages and Figure 9 c shows the atomic ratios. (Table 2 and Fig. 9c). Cobalt and manganese were not detected in point 2, which is iridescent. Some significant marked differences are better revealed by the high-resolution XP-spectra for the different analyzed points on this sample.

The first one involves the Fe 2p peak, which showed a different distribution of Fe (II) and Fe (III) in the two points (Fig. 10a). In point 1 the Fe (II) component is more pronounced than in the altered one (point 2); in the altered area on the contrary the iron oxy-hydroxide component is the most abundant Fe species. This finding is substantiated by the O 1s peak, which showed a marked difference on its components in the different points (Figure 10 b). O 1s is a multicomponent peak: the signal at 530.2 eV is due to oxygen in oxides, the one at 531.5 eV is assignable to -OH [43] and to non-bridging oxygen in silicates, and the component at the highest binding energy values (532.3 eV) is ascribed to bridging oxygen in silicates. In the point 2, the second component is the most intense, confirming the larger presence of -OH in this area than in the unaltered one. The most intense photoelectron signal assigned to Mn2p also allows the identification of the chemical state of this element, which is found to be Mn^{4+} (see figure S.2 in supplementary information).

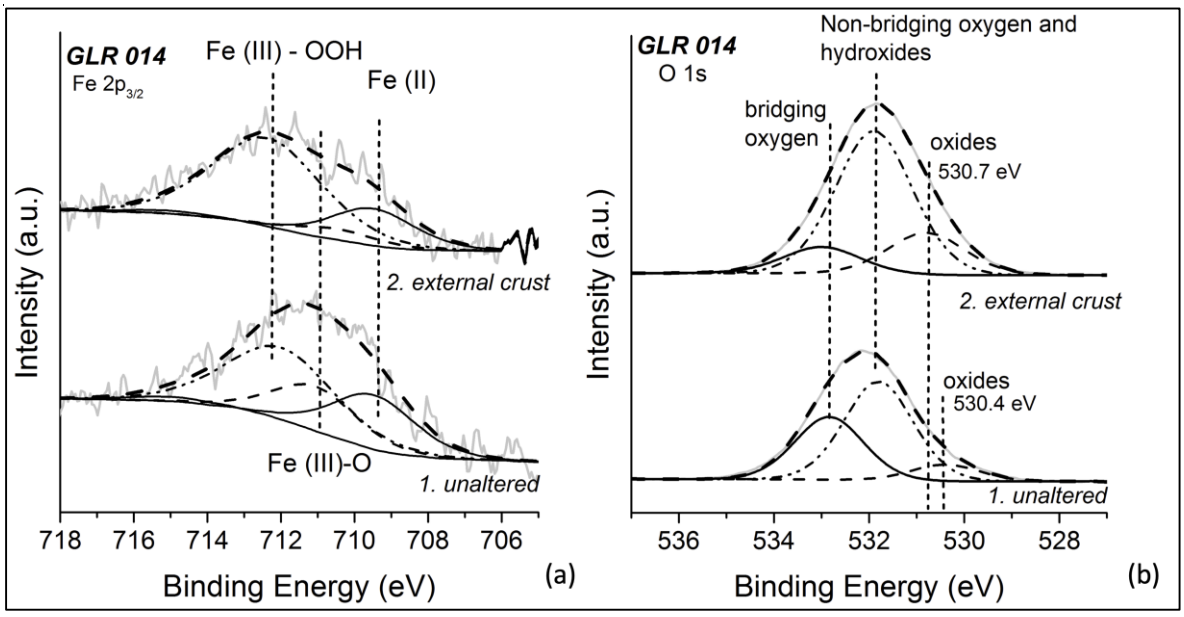

Figure 10. Fe $2p_{3/2}$ peaks recorded points 1 and 2 of sample GLR 014 (a and b respectively) as well as the O 1s peaks recorded in of sample GLR 014 (a and b respectively).

Another impressive difference is related to the carbon components: carbon is always present in all the samples in contact with the atmosphere, as an organic contamination layer. In point 1, C 1s peak showed also an intense peak due to carbonate (Fig. S.3a); the intensity of such component dramatically decreases in point 2 (Fig. S.3b).

3.4 LA-ICP-MS

Two samples (GLB002 and GLU034) were analysed by LA-ICP-MS with the aim to obtain the trace element concentrations (Table 4). For both of them, the analyses were carried out in spot and linear modality (see Materials and Methods paragraph).

Among all analysed elements, Co, Mn, Pb and Ti are the most significant. In particular, comparing the concentrations of altered areas with those measured on the unaltered glass, sample GLU034 shows similar Co concentrations in both portions (iridescent patina and unaltered glass), a decrement of Mn and Ti and an increase of Pb from unaltered glass to iridescent patina. The black encrustation of the GLB002 sample, instead, displays an enrichment in Co, Mn, Pb and Ti.

313 **Table 4.** Average concentration resulted from four analyses by LA-ICP-MS (expressed in ppm) of the most
314 representative chemical elements, both on unaltered and altered glass for samples GLB002 and GlU004 samples.

	GLB002		GLU004	
	Unaltered glass	**Altered glass**	**Unaltered glass**	**Altered glass**
Ti	698	2927	831	561
Mn	9398	19914	518	246
Co	6	27	5	11
Co	6	27	5	11
Cu	24	-	-	-
Cr	121	23	36	32
Ni	11	211	5	6
Pb	15	150	11	68

315

316 **4. Discussion**

317 It is acknowledged that ancient glasses exposed for long time to unfavorable conditions undergo
318 transformations and alterations. The degradation processes strongly depend on glasses chemical
319 composition and environmental parameters (such as soil humidity, temperature and pH). Exchange
320 reactions take place between the so-called network modifier ions (Na^+, K^+, Ca^{2+} and Mg^{2+}), added to
321 the raw materials in the form of oxides or carbonates to decrease the melting point and making the
322 glass more resistant towards chemical attack and water [37].
323 It has to be noticed that this study area in Northern Africa is subject to the semi-arid Mediterranean
324 climate with few rainfalls, although the site of Aïn Wassel in the Arkou valley has a sub-humid
325 microclimate. Soils are in general clayey, but permeable enough. Worth to note in the region is also
326 the presence of salt originated from the weathering of local diapiric structures, which erodes partly
327 the land surface [44-45].
328 Systematic studies on the corrosion of glasses, i.e. the attack of aqueous solutions onto the glass
329 surface, have been often carried out in the literature by means of SEM-EDS [37]. This technique has
330 allowed us to highlight morphological and elemental distribution differences between altered and
331 unaltered areas. In case of iridescent regions an increase of Si and alkali depletion was detected (see
332 samples GLR011 and GLU034).
333 The weathered glass is a complex system characterized by the presence of very fragile
334 multilayered silica, where the number of layers and their thickness depend upon time. The
335 weathering is mainly due to the effect of water that, through the mechanisms of diffusion and ionic
336 exchange, produces a general loss of modifier ions on the surface of glass, generating almost pure
337 silica iridescent layers [46] like those observed for samples GLR011 and GLU034. In general, three
338 different layers can be identified in weathered glasses: the unaltered bulk glass, the gel layer
339 composed by a hydrated silica network (typically samples GLR011 and GLU034), and the layer of
340 corrosion salts externally formed (GLB002).
341 Samples GLU034 and GLR011 (Fig. 2) show the characteristic lamellar structure formed after the
342 leaching process of alkali ions. Elemental analysis of altered and not altered surfaces carried out by
343 SEM-EDS on these samples, has shown that the degraded surface is characterized by alkali depletion
344 and an increase in silica, compared to less unaltered surface.
345 This ion exchange causes the formation of a thin layer near the glass surface, which is relatively
346 enriched in silica and contains low amount of other cations.
347 Alkaline-earth ions (M^{2+}) could also leach out by a similar mechanism. Indeed, often the leaching of
348 Na from soda-silica-lime glass results in the formation of an outer so-called gel layer, mainly

consisting of the remaining glass components (SiO_2 and CaO) [47]. Curious growth rings develop on the surface of the glass. This characteristic phenomenon has been observed for sample GLU034 (Fig. 2). The alteration layer shows the presence of flakes (Fig. 2): in fact, cracks form as the degradation increases, and they become a vehicle for the passage of water for a subsequent attack.

The leaching phase is followed by a corrosion process in which the silicon oxygen bonds (Si-O-Si) are broken. This phenomenon is called glass depolymerization and progresses gradually to greater depths up to 150 μm.

Cracks have been clearly observed for samples GLU034 and GLR011. In particular, in sample GLU034, the presence of craters highlights the beginning of the corrosion process. Many authors describe that the transition from the degradation phase defined as leaching to the corrosion phase, can be highlighted on the surface by observing these typical craters; in fact, over time they tend to widen (as the degradation proceeds) until their complete interconnection [10,14,16,18,23].

The layers produced are fragile and inconsistent and this leads to the thinning of the surface. As degradation proceeds, new effects are produced on the surface, which are formed by interaction with pollutants and carbon and sulfur dioxide, which cause the precipitation of salts on the surface.

Some weathering products can be observed on the glass surface in accordance with what reported in the literature [37]. In particular in our case the presence of $CaCO_3$ has been observed by ATR FTIR (Fig. 1S) together with traces due to organic substances (signals at about 2920 cm^{-1}) in accordance with what described by Schreiner et al. [38] where it is reported that the weathering product could be calcium carbonate or some organic Ca-containing compound.

The development of corrosion crusts complicates the analysis of historical glass pieces and the diagnosis of their deterioration [48].

Contrary to the iridescent areas, where a leaching of alkali and alkaline earth ions causes the modification of the glass network, browning corrosion is due to the migration of Mn, Fe and other metallic ions carried by the attacking aqueous solution, which enter in the glass from the surrounding soil or are depleted from the pristine glass core (this is the case of Mn and Fe) [46]. This is perfectly in accordance with what observed for sample GLB002 where an enrichment mainly in Mn, Fe and Ti has been observed on the encrustations together with an increase in Ca, K, Na, Mg, Al, Cl and S (fig. 5). In this case different compounds could be formed; for example, in the literature Fe (III) oxide and oxide hydrates, insoluble sulphides or manganese dioxide are reported and are in part responsible for the darkening of the glass [49]. Nevertheless, since by SEM-EDS we have carried out elemental analyses, it is difficult to make hypotheses on the chemical nature of the species present on the surface. We can just presume that, for example, the observed increment on the encrustations of S, K, Ca, Na and Cl concentrations in case of sample GLB002 could be due to the formation of sulphates such as syngenite ($K_2SO_4 \cdot CaSO_4 \cdot H_2O$) or of chloride as NaCl in accordance to what observed by Schreiner et al. [38].

From the point of view of the surface morphology, sample GLB002 shows (Fig. 4) the typical features characteristic of corrosion processes [50].

XPS has been already applied in the literature for the characterization of the alteration and corrosion phenomena occurring in Roman glass fragments [51] and for investigating the weathering process of glass surfaces with the formation of corrosion growth rings detected by optical microscope [46].

A comparison has been carried out between EDS and XPS results (Fig.11) in order to highlight differences in the chemical composition of the outermost layers compared to the bulk. At this purpose Ca/Si and Na/Si ratios have been considered (atomic percentages detected by XPS were converted into weight percentage in order to compare the results). For sample GLR011 it is confirmed also for the outermost layer what already observed for the bulk, i.e. a decrease of both Ca/Si and Na/Si ratios in the altered areas confirming the formation on the surface of a silica gel depleted in alkali ions.

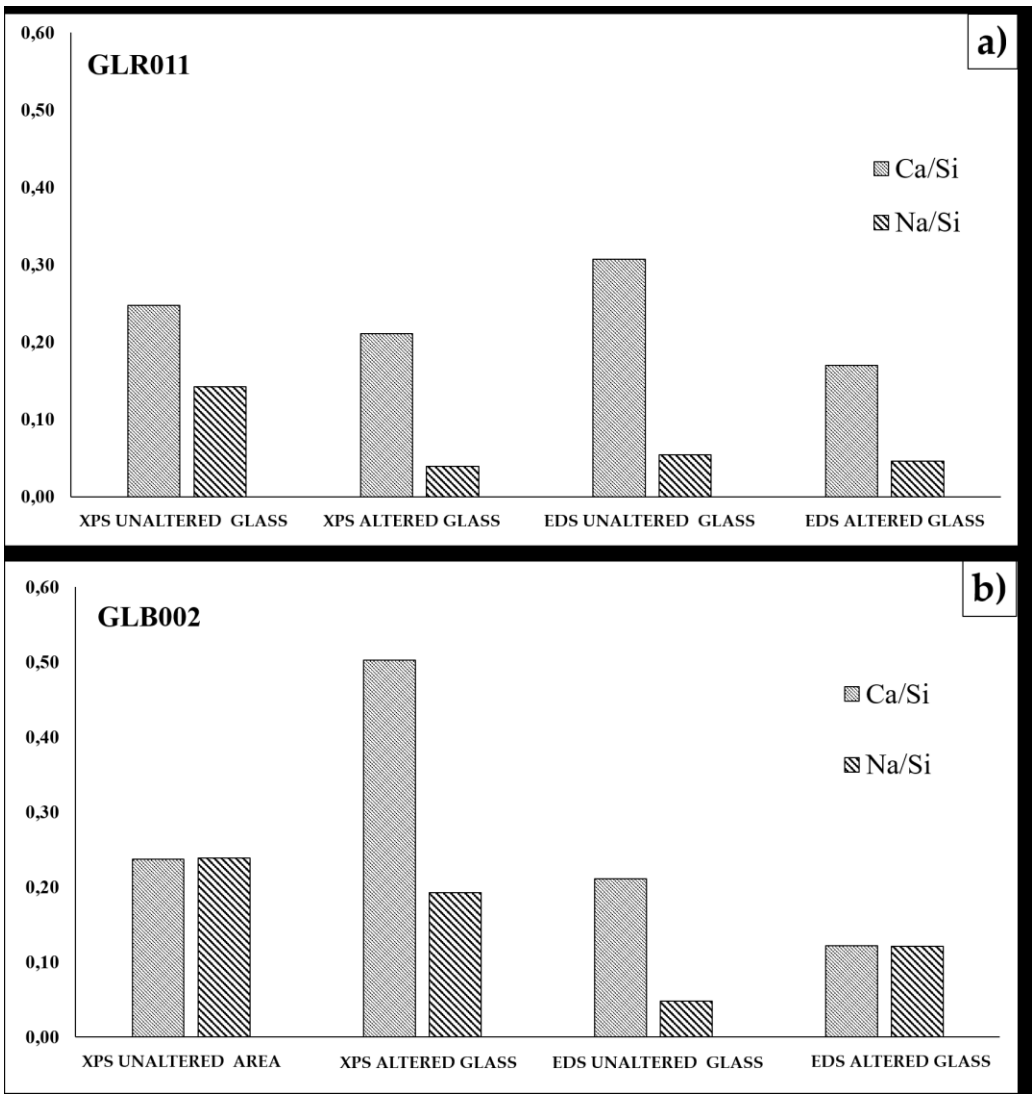

Figure 11. Ca/Si e Na /Si ratios obtained from XPS and EDS analyses carried out on unaltered and altered glass areas for samples GLR011 (a) and GLB002 (b).

The formation of silica gel is confirmed by XPS data: taking into account all the samples, the binding energy of Si 2p increases with sodium and calcium depletion towards values typical of SiO_2 (Fig. 12a). Besides, in O 1s peaks, the component ascribed to non-bridging oxygen increases its intensity in the visibly altered regions, where cation/silicon ratios decrease (Fig. 12b). If the non-bridging /bridging oxygen area ratio (NBO/BO) is plotted *vs* Ca/Si (Fig.12c) and Na/Si (Figure 13d) ratios it is evident that, in the cations depleted areas, NBO/BO increases substantiating the hypothesis of silicate depolymerization. The only exception is represented by point 2 of the GLB002 sample where NBO/BO increases with Ca/Si ratio (Fig12 c). In that area encrustations enriched in $CaCO_3$ have been evidenced: XPS analysis has highlighted how Ca enrichment takes place in the outermost layer (Ca/Si ratio determined by XPS is remarkably higher than that determined by EDS) and the presence of calcium carbonate is in agreement with the FT-IR spectra.

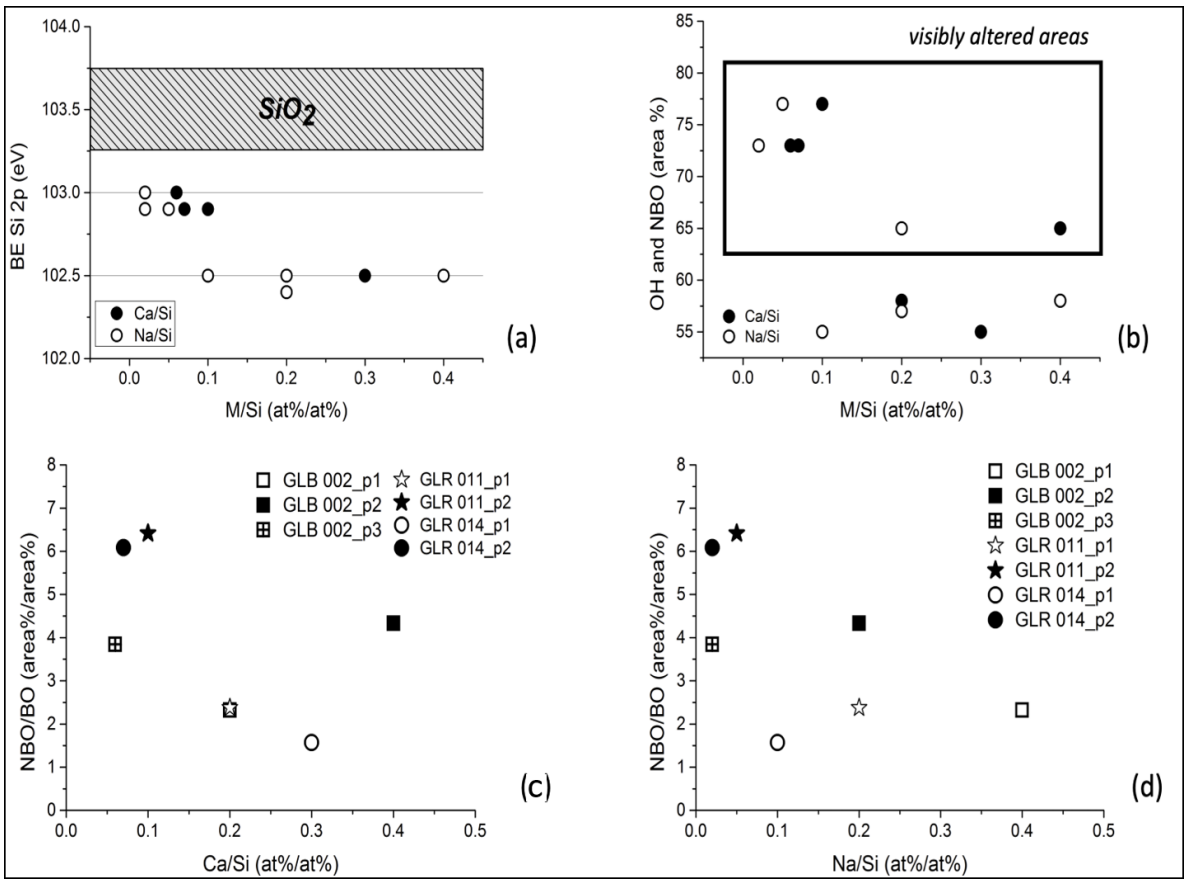

Figure 12. (a) binding energy (BE) of XPS Si 2p peak versus cation/Si ratios. The shaded area represents the range of BE reported in literature for SiO2. [52] [ref: https://srdata.nist.gov/xps/selEnergyType.aspx]; (b) Area % of non-bridging and OH component in O 1s peak vs Ca/Si and Na/Si ratios; (c) non-bridging/bridging oxygen area ratio from O 1s peaks vs Ca/Si ratios and (d) Na/Si ratios.

It is worth noting that also Fe 2p signals recorded in the visibly altered regions of samples GLB002 and GLR014 reflect the higher amount of hydroxides, whose signals in O 1s peaks fall at the same binding energy values of NBO, being the components at about 712 eV more intense in the external encrustations (points 2).

As far as sample GLR014, the presence of an intense component ascribed to carbonate in C 1s signal recorded on point 1, could be due the presence of sodium and calcium carbonate. The marked decrease of sodium, calcium (and also of other metals such as Co and Mn) and of the carbonate component in point 2, could be due to leaching processes.

The LA-ICP-MS results highlight the different enrichment patterns observed in the black encrustation of GLB002 and in the iridescent patina of GLU034. Indeed, the black encrustation of GLB002 compared to the unaltered bulk glass is always enriched in Co, Mn, Ni, Pb and Ti. It is worth mentioning that the Mn and Ti enrichment was also confirmed by SEM-EDS data. Enrichment in Mn has been observed on encrustations also in another study reported in the literature [40].

The iridescent patina of GLU034 sample, compared to the unaltered bulk glass, only shows a higher value of Pb.

Considering that the Pb is calcium-vicariant, his enrichment is coherent with the observed presence of Ca compounds in both samples. Moreover, the higher values of other heavy metals (Co, Ni, Ti) are in agreement with the presence of different compounds (oxide and oxide hydrates, insoluble sulphides or manganese dioxide) and they are jointly responsible for the darkening of the glass [49].

The different chemical behaviour of the two types of degradation layers is evident in the binary diagrams Co versus Mn, Pb versus Mn and Ti versus Pb (Fig. 13) and in the histograms of Figure 14.

The black encrustation of GBL002, instead, is depleted in Cu and Cr. Since the investigations have been performed only on a limited number of samples, advancing explanations for these phenomena might be speculative. Nevertheless, the increase in some elements such as Pb on the altered areas could be explained with depletion in other elements.

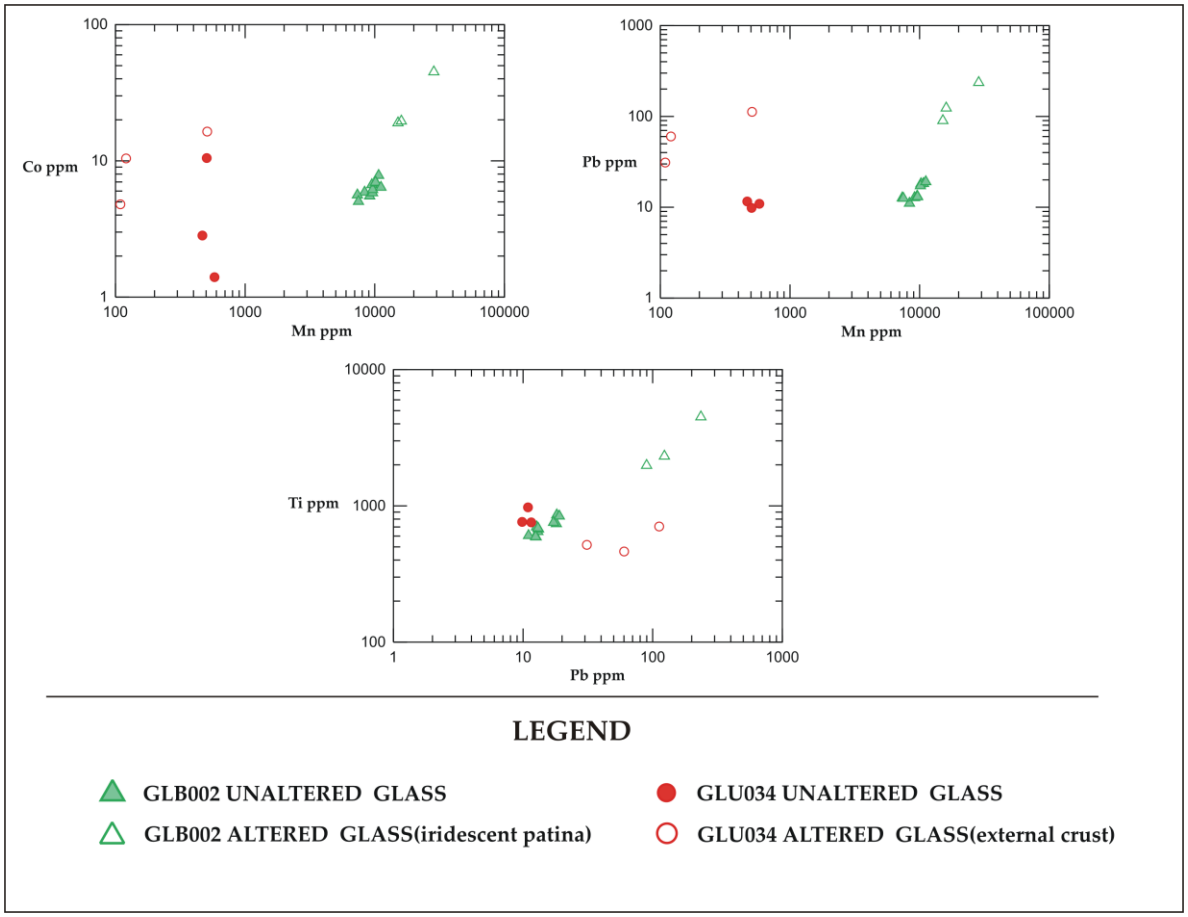

Figure 13. Binary diagrams relative to the concentrations of some trace elements such as: Co vs Mn, Pb vs Mn and Ti vs Pb, detected on different morphological glass areas.

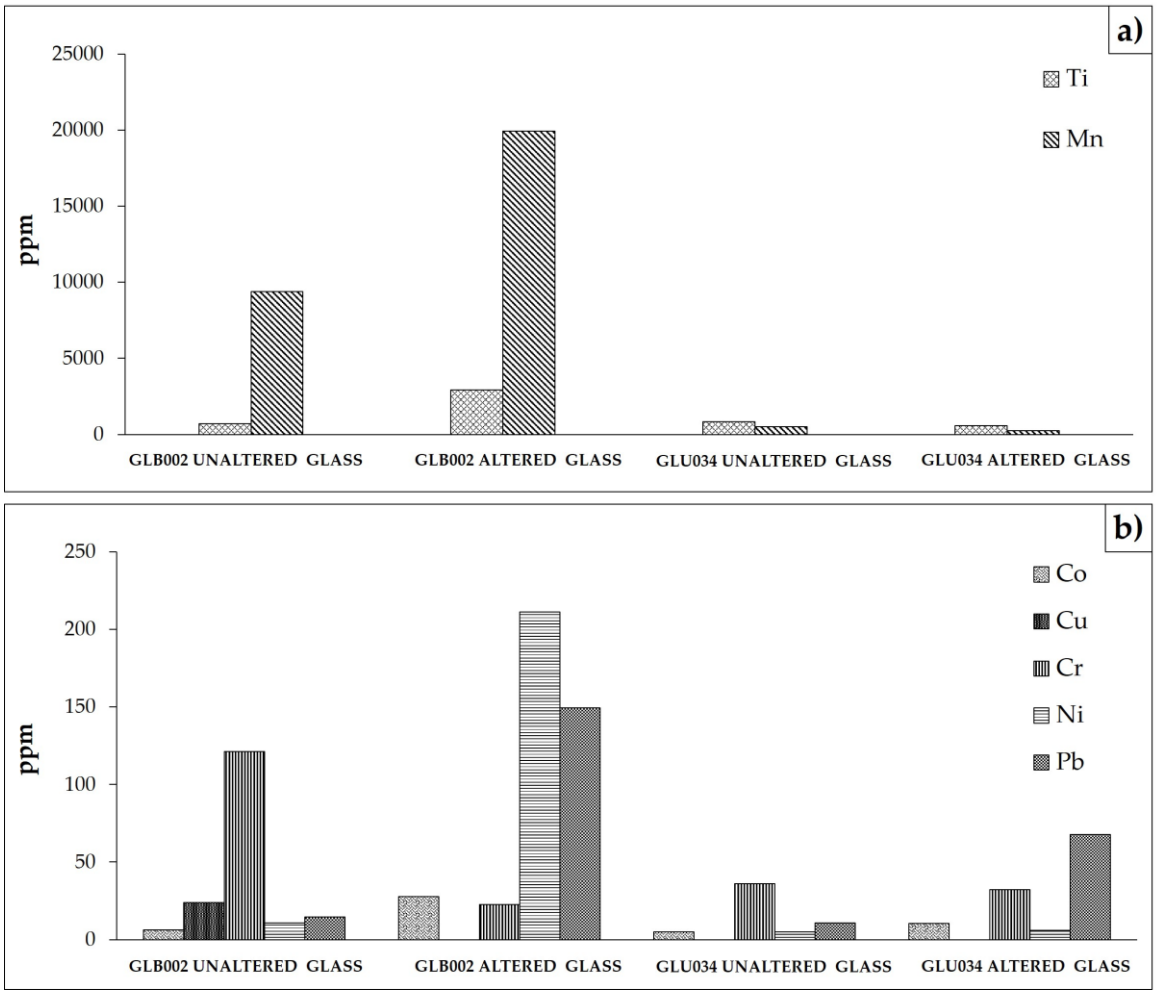

Figure 14. Histograms of a) Mn, Ti; b) Co, Cr, Cu, Ni, Pb in both unaltered and altered areas of GLB002 and GLU034 samples.

5. Conclusions

The present paper is focused on the characterization of the degradation products present on the surface of some Byzantine glass shards. The surface of the investigated samples appears to be differently altered: where alkali depletion occurred together with enrichment in silica the appearance of iridescence is very pronounced in the most damaged areas. On the other hand, the enrichment in Ca or in some other metals, such as for example Mn, was revealed in the case of the encrustations. The applied techniques allowed the identification of the morphology of the differently altered regions on the same sample as well as the elemental composition of the bulk by SEM-EDS. The information obtained by XPS are complementary: the outermost surface and the compounds present in the various points are fully characterized. A technique such as LA-ICP-MS is demonstrated to be particularly useful for quantifying metal in trace amounts and for discriminating the two kinds of degradation phenomena on the base of some binary diagrams.

Supplementary Materials: The following are available online at www.mdpi.com/xxx/s1

Author Contributions: "Conceptualization, P.F. and V.C.; methodology, V.C., A.R., M.F., D.A.; investigation, V.C., M.F. D.B.; data processing, P.F, A.R, M.F., V.G., D. B., M. L.; writing—original draft preparation, P.F., V.C., A.R., M.F., writing—review and editing, P.F, A.R, M.F., V.G., D.A., M. L.; supervision, P.F., A.R., M.A; project administration, P.F.; All authors have read and agreed to the published version of the manuscript."

References

1. Barbera, G., Barone, G., Crupi, V., Longo, F., Majolino, D., Mazzoleni, P., Venuti, V. Study of Late Roman and Byzantine glass by the combined use of analytical techniques. *J Non Cryst Solids*, **2012,** *358(12-13),* 1554–1561.
2. Huisman, D.J., Pols, S., Joosten, I., van Os, B.J.H., Smit, A. Degradation processes in colourless Roman glass: cases from the Bocholtz burial. *J. Archaeol. Sci.,* **2008,** *35 (2),* 398-411.
3. Doménech Carbo, M.T., Doménech Carbò, A., Osete Cortina, L., Saurì Peris, M.C. A Study on Corrosion Processes of Archaeological Glass from the Valencian Region (Spain) and its Consolidation Treatment, *Microchim Acta* 154, **2006,** *123–142.*
4. Carmona, N., Oujja, M., Rebollar, E., Romich, H., Castillejo M. Analysis of corroded glasses by laser induced breakdown spectroscopy. *Spectrochim Acta A,* **2005,** B 60, 1155 – 1162.
5. Gentaz, L., Lombardo, T., Chabas, A., Loisel, C., Verney-Carron, A. Impact of neocrystallisations on the SiO_2-K_2O-CaO glass degradation due to atmospheric dry depositions. *Atmos. Environ*. **2012,** *55,* 459-466.
6. Palomar, T., Oujja, M., García-Heras, M., Villegas, M.A., Castillejo, M. Laser induced breakdown spectroscopy for analysis and characterization of degradation pathologies of Roman glasses. *Spectrochim Acta Part B At Spectrosc*, **2013,** *87,* 114-120.
7. Melcher, M., Wiesinger, R., Schreiner, M. Degradation of glass artifacts: Application of modern surface analytical techniques. *Acc. Chem. Res.* **2010,** *43 (6),* 916-926.
8. Palomar Sanz, T. Effect of soil pH on the degradation of silicate glasses. *Int J Appl Glass Sci.* **2017**; *8,* 177–187.
9. Jackson, C.M., Greenfield, D., Howie, L.A. An assessment of compositional and morphological changes in model archaeological glasses in an acid burial matrix *Archaeometry,* **2012**, *54 (3),* 489-507.
10. Licenziati, F., Falcone, R., Orsega, E.F., Marco Verità Studio preliminare sulla produzione e il degrado di vetri potassici e sodici come modelli di vetrate artistiche e di vetri industriali in ambiente confinato. *Rivista della Stazione Sperimentale del Vetro* **2010,** *3,* pp. 7-17.
11. Terreni, L.G. Le problematiche conservative del vetro antico proveniente da scavi archeologici. *Rivista Millarium,34-47.*
12. Silvestri, A., Molin, G., Salviulo, G. Roman and medieval glass from the Italian area: bulk characterisation and relationships with production technologies, *Archaeometry* **2005,** *47 (4),* 797–816.
13. Verità, M. Analisi di reperti vitrei e scarti di lavorazione di tarda età romana provenienti dagli scavi del monastero di Santa Giulia a Brescia. In *Santa Giulia di Brescia: gli scavi dal 1980 al 1992,* Brogiolo, G.P., Morandini, F., Rossi, F. Eds.; Reperti preromani, romani e altomedievali All'Insegna dell'Giglio, Publisher: Firenze, Italia, 1999, pp. 309–314.
14. Werner V., *Glass chemistry,* 2nd Publisher: Springer Berlin Heidelberg, New York, Berlin, 1994.
15. Scholze, H., *Glass nature, structure and properties,* Publisher: Springer Verlag, New York, 1991.
16. Verità M., *Modern and ancient glass: nature, composition and deterioration mechanisms, The Materials of Cultural Heritage in their Environment, Centro Universitario per i Beni culturali, Ravello,* Publisher:EdiPuglia, Bari 2006.
17. Davison, S., Newton R., *Conservation and Restoration of Glass,* 2nd ed., Publisher: Butterworth- Heinemann Ed., Oxford, 2007.
18. Das, C.R., Douglas, R.W. Studies on the reaction between water and glass. Part 3. *Phys. Chem.* **1967,** *8, 5,* 178-184.
19. Varshneya K., *Fundamentals of inorganic glass,* Ed. Academic Press, New York,1993.
20. Walters, H.V., Adams, P.B., Effects of Humidity on the weathering of glass, *J Non Cryst Solids*, **1975,** *19,* 183-199.
21. Munier, I., Lefèvre, R.A., Losno, R. Atmospheric factors influencing the formation of Neocrystallisation on low durability glass expose to urban atmosphere, *Glass Technol*, **2002,** *43, C,* 114-124.
22. Geotti-Bianchini, F., and Preo, M., *Fattori rilevanti per prevenire alterazione idrolitica ("ossidazione") del vetro Float,* Rivista della Stazione Sperimentale del Vetro, 1999, 3, 127- 140.
23. Bianchini-Geotti F., Nicola C., Preo M., Vallotto M., Verità M., *MicroIRRS and EPMA study of the weathering of potash-lime-silicate glasses,* Rivista della Stazione Sperimentale del Vetro, 2005, 3, 49-61.
24. Munier, I.; Lefèvre, R.A.; Geotti-Bianchini, F.; Verità, M., Influence of polluted urban atmosphere on the weathering of low durability glasses. *Glass Technol-Part A,* **2002,** *43, 6,* 225-237.
25. Falcone, R., Nardone, M., Sodo, A., Sommariva, G., Vallotto, M., Verità M. SEM-EDS, EPMA and MRS analysis of neo-crystallisations on weathered glasses, *Mater. Sci. Eng. 2010*, *7,* 1-7.

26. Lombardo, T., Chabas, A., Lefevre, R.A., Verità, M., Geotti-Bianchini, F. Weathering of a float glass exposed outdoor in urban area, *Glass Technol*, **2005,** 46, 271-276.
27. Verità, M., Falcone, R., Sommariva, G., Chopinet, M.H, Lehuédé, P., Weathering of the inners surface of soda-lime-silica glass containers exposed to the atmosphere, *Glass Technol-Part A,* **2009,** 50,1, 65-70.
28. Fermo, P., Andreoli, M., Bonizzoni, L., Fantauzzi, M., Giubertoni, G., Ludwig, N., Rossi, A. Characterisation of Roman and Byzantine glasses from the surroundings of Thugga (Tunisia): Raw materials and colour. *Microchem J,* **2016,** *129,* 5-15.
29. Andreoli, M., Glass finds from a Late Antique-Byzantine farm at Aïn Ouassel (Tunisia). *Antiquités africaines*, **2015,** *51,* 219-233.
30. Andreoli, M., Reperti vitrei. In Rus Africum IV. La fattoria Bizantina di Aïn Wassel, Africa Proconsularis (Alto Tell, Tunisia), Raaijmakers deVos, M., Maurina, B. Eds. Publisher: Archaeopress, Oxford, England, 2019, pp. 302-312.
31. Cappelletti, G., Ardizzone, S., Fermo, P., Gilardoni, S. The influence of iron content on the promotion of the zircon structure and the optical properties of pink coral pigments. *J. Eur. Ceram*., **2005,** *25 (6),* 911-917.
32. Gunther, D., Heinrich, C.A. Enhanced sensitivity in laser ablation-ICP mass spectrometry using helium-argon mixtures as aerosol carrier. *Journal of Analytical Atomic Spectrometry* **1999**, *14,* 1363-1368.
33. Barca, D., M. Abate, G.M. Crisci, De Presbiteris, D. Post-Medieval glass from the castle of Cosenza, Italy: chemical characterization by LA-ICP-MS and SEM-EDS, *Per. Min*., **2009,** *78 (2),* 49–64.
34. Barca, D., Basso, E., Bersani, D., Galli, G., Invernizzi, C., La Russa, M.F., Lottici, P.P., Malagodi, M., Ruffolo S.A. Vitreous tesserae from the calidarium mosaics of the Villa dei Quintili, Rome. Chemical composition and production technology. *Microchem J,* **2016,** *124,* 726-735.
35. Barca, D., Papparella, F.C. Chemical, characterization of vitreous finds from Cosenza cathedral (Calabria - Italy) by the combined use of analytical techniques. *Archaeology* **2020;** *6,* 63–85.
36. Fiorenza, E., Rovella, N., D'andrea, M., Musella, M., Sudano, F., Taliano Grasso, A., Barca D. Vitreous tesserae from the Four Seasons Mosaic of S. Aloe quarter in Vibo Valentia – Calabria, Italy: a chemical characterization. *Minerals* **2020,** *10,* 65-85.
37. Schreiner, M., Melcher, M., Uhlir, K. Scanning electron microscopy and energy dispersive analysis: Applications in the field of cultural heritage. *Anal. Bioanal. Chem.* **2007,** *387 (3),* 737-747.
38. Bonizzoni, L., Bruni, S., Guglielmi,V., Milazzo, M., Neri, O. Field and laboratory multi-technique analysis of pigments and organic painting media from an Egyptian coffin (26th dynasty). *Archaeometry,* **2011,** *53, 6,* 1212–1230.
39. Bruni, S., Guglielmi, V., Della Foglia, E., Castoldi, M., Bagnasco G. A non-destructive spectroscopic study of the decoration of archaeological pottery: from matt-painted bichrome ceramic sherds (southern Italy, VIII-VII B.C.) to an intact Etruscan cinerary urn. *Spectrochim Acta A,* **2018,** *191, 88-97.*
40. Palomar Sanz, T.; García Heras, M.; Sáiz-Jiménez, C.; Márquez Goncer, C.; Villegas Broncano, M.Á. Technical Note: Pathologies and analytical study of mosaic materials from Carmona and Italica. *Mater. de Construccion,* **2011,** *61, 304,* 629-636. doi: 10.3989/mc.2011.64310
41. Abd-Allah R. Chemical cleaning of soiled deposits and encrustations on archaeological glass: a diagnostic and practical study. *J Cult Herit.* **2013**; *14,* 97–108.
42. Palomar, T., Garcia Herasa, M, Sabiob, R., Rinconc, J.M., Villegasa, M.A. Composition, preservation and production technology of Augusta Emerita roman glasses from the first to the sixth century AD. *Mediterr. Archaeol. Archaeom*. **2012,** *12, 2,* 193-211.
43. Fantauzzi, M., Pacella, A., Atzei, D., Gianfagna, A., Andreozzi, G.B., Rossi, A. Combined use of X-ray photoelectron and Mössbauer spectroscopic techniques in the analytical characterization of iron oxidation state in amphibole asbestos. *Anal. Bioanal. Chem*., **2010,** *396 (8),* 2889-2898.
44. de Vos, M., Terra acqua e olio nell'Africa settentrionale. Scavo e ricognizione nei dintorni di Dougga (Alto Tell tunisino). Ed., Rus Africum. Publisher: Temi, Trento, Italia, 2000.
45. Raaijmakers deVos, M., Maurina, B., *La fattoria Bizantina di Aïn Wassel, Africa Proconsularis (Alto Tell, Tunisia).* Eds, Rus Africum IV. Publisher: Archaeopress, Oxford, England, 2019.
46. Dal Bianco, B., Bertoncello, R. The development of growth rings on ancient glass surfaces: Description and simulation of the weathering. *J Non Cryst Solids* **2008,** *354 (2-9),* 773-779.
47. Newton, R.G., The durability of glass, a review. *Glass Technol,* **1984,** 26, 21-38.
48. Carmona, N., Oujja, M., Rebollar, E., Römich, H., Castillejo, M. Analysis of corroded glasses by laser induced breakdown spectroscopy. *Spectrochim. Acta B,* **2005,** *60 (7-8),* 1155-1162.

49. Doménech-Carbó, M.-T., Doménech-Carbó, A., Osete-Cortina, L., Saurí-Peris, M.-C. A study on corrosion processes of archaeological glass from the Valencian Region (Spain) and its consolidation treatment. *Microchimica Acta*, **2006**, *154 (1-2), 123-142*.
50. Tournié, A., Ricciardi, P., Colomban, Ph. Glass corrosion mechanisms: A multiscale analysis. *Solid State Ionics*, **2008**, 179 (38), pp. 2142-2154.
51. Barbana, F., Bertoncello, R., Milanese, L., Sada, C. Alteration and corrosion phenomena in Roman submerged glass fragments. *J Non Cryst Solids,* **2004,** *337 (2),* 136-141.
52. Retrieve data for a selected element. Available online: https://srdata.nist.gov/xps/selEnergyType.aspx (21/09/2020).